Biochemical Pharmacology 195 (2022) 114850

Contents lists available at ScienceDirect

Biochemical Pharmacology

journal homepage: www.elsevier.com/locate/biochempharm

Differential contribution of renal cytochrome P450 enzymes to kidney endothelial dysfunction and vascular oxidative stress in obesity

Mercedes Muñoz [a,1], Elvira López-Oliva [a,1], Estéfano Pinilla [a,2], Claudia Rodríguez [a,2], María Pilar Martínez [b,2], Cristina Contreras [a], Alfonso Gómez [a], Sara Benedito [a], Javier Sáenz-Medina [c], Luis Rivera [a,*], Dolores Prieto [a,*]

[a] Departamento de Fisiología, Facultad de Farmacia, Universidad Complutense, Madrid, Spain
[b] Departamento de Anatomía y Embriología, Facultad de Veterinaria, Universidad Complutense, Madrid, Spain
[c] Departamento de Urología, Hospital Universitario Puerta de Hierro-Majadahonda, Madrid, Spain

ARTICLE INFO

Keywords:
CYP2C epoxygenases
CYP4 hydroxylase
Endothelial dysfunction
Reactive oxygen species
Kidney preglomerular arteries
Obesity

ABSTRACT

Arachidonic acid (AA)-derived cytochrome P450 (CYP) derivatives, epoxyeicosatrienoic acids (EETs) and 20-hidroxyeicosatetranoic acid (20-HETE), play a key role in kidney tubular and vascular functions and blood pressure. Altered metabolism of CYP epoxygenases and CYP hydroxylases has differentially been involved in the pathogenesis of metabolic disease-associated vascular complications, although the mechanisms responsible for the vascular injury are unclear. The present study aimed to assess whether obesity-induced changes in CYP enzymes may contribute to oxidative stress and endothelial dysfunction in kidney preglomerular arteries. Endothelial function and reactive oxygen species (ROS) production were assessed in interlobar arteries of obese Zucker rats (OZR) and their lean counterparts lean Zucker rats (LZR) and the effects of CYP2C and CYP4A inhibitors sulfaphenazole and HET0016, respectively, were examined on the endothelium-dependent relaxations and $O_2^{\bullet-}$ and H_2O_2 levels of preglomerular arteries. Non-nitric oxide (NO) non-prostanoid endothelium-derived hyperpolarization (EDH)-type responses were preserved but resistant to the CYP epoxygenase blocker sulfaphenazole in OZR in contrast to those in LZR. Sulfaphenazole did not further inhibit reduced arterial H_2O_2 levels, and CYP2C11/CYP2C23 enzymes were downregulated in intrarenal arteries from OZR. Renal EDH-mediated relaxations were preserved in obese rats by the enhanced activity and expression of endothelial calcium-activated potassium channels (K_{Ca}). CYP4A blockade restored impaired NO-mediated dilatation and inhibited augmented $O_2^{\bullet-}$ production in kidney arteries from OZR. The current data demonstrate that both decreased endothelial CYP2C11/ CYP2C23-derived vasodilator H_2O_2 and augmented CYP4A-derived 20-HETE contribute to endothelial dysfunction and vascular oxidative stress in obesity. CYP4A inhibitors ameliorate arterial oxidative stress and restore endothelial function which suggests its therapeutic potential for the vascular complications of obesity-associated kidney injury.

1. Introduction

Arachidonic acid (AA)-derived cytochrome P450 (CYP) metabolites, epoxyeicosatrienoic acids (EETs) and 20-hidroxyeicosatetranoic acid (20-HETE) play a key role in kidney metabolism and are involved in the regulation of both renal tubular and vascular functions and blood

Abbreviations: AA, arachidonic acid; ACh, acetylcholine; CYP, cytochrome P450; COX, cyclooxygenase; CKD, chronic kidney disease; EC, endothelial cell; EDH, endothelium-derived-hyperpolarization; EETs, epoxyeicosatrienoic acids; 20-HETE, 20-hidroxyeicosatetranoic acid; eNOS, endothelial nitric oxide synthase; H_2O_2, hydrogen peroxide; K_{Ca} channel, calcium-activated potasium channel; $K_{Ca}2.3$ channel, small conductance K_{Ca} channel; $K_{Ca3.1}$, intermediate conductance K_{Ca} channel; LZR, lean Zucker rats; NADPH, nicotinamide adenine dinucleotide phosphate; NF-κB, nuclear factor kappa-light-chain-enhancer of activated B cells; NO, nitric oxide; NOS, nitric oxide synthase; Nox, NADPH oxidase enzymes; $O_2^{\bullet-}$, superoxide; OZR, obese Zucker rats; Phe, phenylephrine; PSS, physiological saline solution; RIAECs, rat intrarenal artery endothelial cells; ROS, reactive oxygen species; TNFα, tumor necrosis factor alfa; VSM, vascular smooth muscle.

* Corresponding author at: Departamento de Fisiología, Facultad de Farmacia, Universidad Complutense de Madrid, 28040 Madrid, Spain.
E-mail address: dprieto@ucm.es (D. Prieto).

[1] Equal contribution.
[2] Equal contribution.

https://doi.org/10.1016/j.bcp.2021.114850
Received 18 October 2021; Received in revised form 17 November 2021; Accepted 18 November 2021
Available online 22 November 2021

pressure [1,2]. CYP enzymes are highly expressed in tubular epithelial cells and synthesize EETs and HETEs that participate in the regulation of sodium tubular transport [2]. However, CYP epoxygenases and CYP hydroxylases are also found in renal endothelial and other kidney vascular cells and are involved in the local control of renal blood flow. Thus, 20-HETE is a potent vasoconstrictor of renal afferent arterioles that participates in blood flow autoregulation, whereas EETs actions include vasodilation, anti-inflammation, anti-fibrosis and anti-apoptosis in the kidney, and also in heart and blood vessels [1,3,4,5]. EETs were early proposed as endothelial-derived hyperpolarizing (EDH) factors and CYP2C epoxygenase as an EDHF synthase involved in the relaxations of small arteries [4,6,7]. In the coronary endothelium, CYP2C enzymes were reported to be a source of vasoconstrictor superoxide ($O_2^{\bullet-}$) that modulates endothelium-dependent vasodilatation [8]; in contrast, in renal endothelial cells our group has demonstrated that CYP2C11 and CYP2C23 epoxygenases are highly expressed co-localized with eNOS and generate hydrogen peroxide (H_2O_2) as a by-product that is involved in the EDH-type relaxations of kidney preglomerular arteries [9].

Obesity and metabolic syndrome increase the risk for diabetic nephropathy and chronic kidney disease (CKD), although it is now well stablished that obesity *per se* is a risk factor for CKD independent of diabetes, hypertension and other comorbidities [10,11]. The global increase in CKD parallels the obesity global epidemy, and microalbuminuria that further progresses to overt albuminuria, is the earliest sign of obesity-associated vascular dysfunction [11]. Altered metabolism of CYP enzymes has differentially been involved in the pathogenesis of metabolic disease vascular complications. Thus, increased activity of soluble epoxide hydrolase (sEH), the enzyme hydrolyzing EETs, and decreased levels of EETs have been reported to underlie diabetic nephropathy and to contribute to progressive renal damage, sEH gene deletion improving afferent renal arteriole endothelial function and reducing renal injury in streptozotocin-induced diabetes [12,13]. Down-regulation of CYP2C epoxygenases was found in renal and mesenteric microvessels of genetically obese Zucker rats associated to impaired vasodilatation [14,15,16], while endothelial CYP epoxygenase overexpression has been reported to attenuate acute vascular inflammation induced by endotoxin-elicited activation of nuclear factor (NF)-κB signalling [3].

On the other hand, 20-HETE has been reported to underlie diabetes and obesity-related cardiovascular and metabolic disorders and increased circulating and adipose levels of 20-HETE have been involved in high fat diet (HFD)-induced obesity, impaired insulin signalling and insulin resistance [17]. Moreover, highly elevated levels of 20-HETE in large conduit arteries have been associated with impaired elastin degradation and artery compliance, and increased blood pressure in animal models of metabolic syndrome [18], and also in metabolic syndrome-associated coronary endothelial dysfunction [19].

In the kidney, H_2O_2 derived from endothelial CYP2C11 and CYP2C23 epoxygenases contributes to the EDH-type vasodilator responses of preglomerular arteries [9]. Obesity is associated with renal endothelial dysfunction involving oxidative stress from COX-2, NADPH oxidases (Nox) and xanthine oxidase, impaired NO-mediated vasodilatation and reduced H_2O_2 vascular levels [14,20,21,22]. We hypothesized here that altered CYP metabolism contributes to endothelial and vascular dysfunction in intrarenal arteries in obesity and aimed to assess whether obesity-induced changes in CYP epoxygenases and CYP hydroxylases contribute to oxidative stress and endothelial dysfunction in kidney arteries.

2. Materials and methods

2.1. Animal model

Animal care and experimental procedures were in compliance with the European Union Guidelines for the Care and the Use of Laboratory Animals (European Union Directive 2010/63/EU) and were approved by Animal Protection Area of Comunidad de Madrid (Ref PROEX 192.3/20). In the present study, male obese Zucker rats (OZR) (fa/fa) and control lean Zucker rats (LZR) (fa/-) aged 8–10 weeks were purchased from Charles River Laboratories (Barcelona, Spain) and were used for the study at 16–18 weeks age. At this age, OZR were heavier than LZR and exhibited mild hyperglycemia, hyperlipidemia and hypercholesterolemia (Table 1). After sacrifice, kidneys were placed in cold (4 °C) physiological saline solution (PSS) containing (mM): NaCl 119, $NaHCO_3$ 25, KCl 4.7, KH_2PO_4 1.17, $MgSO_4$ 1.18, $CaCl_2$ 1.5, EDTA 0.027 and glucose 11, continuously bubbled with 5% CO_2 in O_2 to maintain pH at 7.4.

2.2. Dissection and mounting of microvessels

Renal interlobar arteries, 2nd–3rd order branches of the renal artery, were dissected from LZR and OZR kidney by removing medullary connective tissue. Arterial segments 2 mm long were mounted in parallel in double microvascular myographs (Danish Myotechnology, Denmark) to measure isometric force, and equilibrated for 30 min in the myograph chamber filled with PSS and maintained at 37 °C. For each individual artery, the relationship between passive wall tension and internal circumference L_{100} corresponding to a transmural pressure of 100 mmHg for a relaxed vessel *in situ* was calculated. The arteries were set to L_1 equal to 0.9 times L_{100} ($L_1 = 0.9 \times L_{100}$), since force development is close to maximal at this internal circumference.

2.3. Experimental procedures for the functional assays

Arteries were first stimulated twice with 120 mM K^+ (KPSS) to test vessel viability. Endothelium-dependent vasodilatation of interlobar arteries was assessed by the relaxations to cumulative concentrations of acetylcholine (ACh) in arteries precontracted with phenylephrine (Phe) (0.1–0.5 μM) and previously incubated with L-NOARG (100 μM) (Sigma-Aldrich, Spain) and indomethacin (1 μM) (Sigma-Aldrich, Spain) to block NOS and COX enzymes, respectively. The relaxant responses to exogenous ACh were then assessed in a second curve after treatment with the specific inhibitor of CYP2C epoxygenases 4-amino-N-(1-phenyl-1*H*-pyrazol-5-yl) benzenesulfonamide (sulfaphenazole, 1 μM) [23] (Sigma-Aldrich, Spain), the selective blockers of $K_{Ca}3.1$ channels (TRAM 34, 1 μM) (Sigma-Aldrich, Spain) and $K_{Ca}2.3$ channels (UCL 1684, 0.3 μM) (Sigma-Aldrich, Spain) and the selective inhibitor of the 20-HETE synthesizing enzymes CYP4A and CYP4F, N-Hydroxy-N′-(4-butyl-2-methylphenyl) formamidine (HET0016, 1 μM) [24] (Sigma-Aldrich, Spain). Drugs were added to the myograph chamber 30 min before the second curve to ACh was performed and Phe concentration was adjusted to match the contraction during the first control curve.

2.4. Measurement of superoxide production by chemiluminescence

Basal and NADPH-stimulated levels of superoxide were detected by lucigenin-enhanced chemiluminiscence in samples of kidney arteries and renal cortex, as previously described [21,22,25]. Cortex samples and 4–5 mm long segments of renal interlobar arteries were dissected

Table 1
Metabolic parameters of LZR and OZR.

	LZR	*n*	*OZR*	*n*
Body weight (g)	373 ± 9	14	449 ± 11***	18
$[Glucose]_{blood}$ (mg/dl)	102 ± 8	12	140 ± 9*	13
$[Cholesterol]_{plasma}$ (mg/dl)	93 ± 4	12	192 ± 13***	13
$[Triglycerides]_{plasma}$ (mg/dl)	83 ± 7	12	313 ± 33***	13

Data are means ± SEM of the number *n* of animals. Significant differences were analyzed by an unpaired Student *t*-test. * $p < 0.05$; **$p < 0.001$; *** $p < 0.0001$ *vs* LZR.

out from the kidneys of each OZR and LZR, equilibrated in PSS for 30 min at room temperature and then some of them were incubated with the CYP2C inhibitor sulfaphenazole (1 μM), the non-selective NADPH oxidase inhibitor apocynin (30 μM) and the 20-HETE biosynthesis inhibitor HET0016 (1 μM) for 30 min at 37 °C to assess the relative contribution of the different CYP enzymes to NADPH-dependent ROS generation. Cortex samples and arteries and were then transferred to microtiter plate wells containing 5 μM bis-N-methylacridinium nitrate (lucigenin) (Sigma-Aldrich, Madrid, Spain) in the absence and presence of different ROS sources inhibitors and of stimulation with NADPH which was added previously to determination in air-equilibrated Krebs solution buffered with 10 mM HEPES-NaOH. Chemiluminescence was measured in a luminometer (BMG Fluostar Optima). Baseline values were subtracted from the counting values under the different experimental conditions for calculation and superoxide production was normalized to dry tissue weight.

2.5. Measurement of hydrogen peroxide by Amplex Red

H_2O_2 production was measured by Amplex Red H_2O_2 assay Kit (Invitrogen, Thermo Fisher Scientific ES, Madrid, Spain) in renal arteries and in renal cortex [22,25]. Cortex samples and interlobar arteries segments about 4–5 mm long from OZR and LZR were equilibrated in HEPES- PSS for 30 min at room temperature. To determine the relative contribution of CYP2C enzymes to H_2O_2 production, renal tissues samples were incubated in the absence (controls) and presence of the CYP2C inhibitor sulfaphenazole (1 μM) for 30 min at 37 °C and then transferred to microtiter plate black wells containing final concentration of Amplex Red (10 mM) and final concentration of horseradish peroxidase (10 U/ml). Some samples were stimulated with NADPH just prior to determination. Fluorescence was measured in a fluorimeter (BMG Fluostar Optima), using an excitation filter of 544 nm and an emission filter of 590 nm. Background fluorescence was subtracted from the counting values and hydrogen peroxide levels were normalized to dry tissue weight.

2.6. Simultaneous measurements of intracellular Ca^{2+} ($[Ca^{2+}]_i$) and tension

Simultaneous measurements of $[Ca^{2+}]_i$ and tension were performed in intact renal preglomerular arteries by Fura2-AM fluorescence as previously described [9]. Arterial segments from LZR and OZR were incubated in the dark in PSS containing 4 μM Fura-2-AM (Invitrogen, Thermo Fisher Scientific ES, Madrid, Spain) and 0.05% Cremophor EL, for 90 min at 37 °C, washing three times in PSS and changing the solution to PSS with fresh Fura-2-AM after 45 min. The myograph was mounted on an inverted microscope (Zeiss Axiovert S100 TV) equipped for dual excitation wavelength microfluorimetry (Deltascan, Photon Technology International). Arteries were alternately illuminated at 340 and 380 nm wavelengths using a monochromator-based system (Deltascan, PTI) and fluorescence emission intensity was collected through a 510 nm filter using photomultiplier and monitored together with force. Ca^{2+}-insensitive signals were determined after quenching with 25 mM Mn^{2+}, and the values obtained were subtracted from those obtained throughout the experiment. The ratio of fluorescence *F*340/*F*380 corrected for autofluorescence was taken as a measure of $[Ca^{2+}]_i$. Cumulative concentration–response curves to ACh (10^{-8}–10^{-5} M) under conditions of NOS and COX inhibition in the absence and presence of catalase (200 U/mL) were performed in renal arteries pre-contracted with Phe.

2.7. Patch-clamp experiments

Rat interlobar arteries were open longitudinally and then incubated in trypsin/EDTA (0.25%/0.02%) in PBS without Ca^{2+}/Mg^{2+} (Biochrom KG, Berlin, Germany) at 37 °C for 30 min. After that, rat intrarenal artery endothelial cells (RIAECs) were scraped and aspirated from the luminal surface using a pipette tip, seeded on a μ-Dish35 mm low (ibidi GmbH, Gräfelfing, Germany), and perfused (0.5 ml/min) at room temperature (21–25 °C) with extracellular solution. Freshly isolated cells maintained at 4 °C and used for electrophysiological recordings within 4 h after isolation procedure [26].

Voltage-clamp recordings were carried out under the whole-cell configuration using an Axon Multiclamp 700A amplifier (Axon instruments, Molecular Devices, CA, USA) [26,27]. Patch pipettes were made of borosilicate glass capillaries (World Precision Instruments, FL, USA) and the tips polished using a microforge MF-830, achieving a final resistance of 4–7 MΩ. The extracellular solution was composed of (in mmol/L): 140 NaCl, 5 KCl, 1 $MgSO_4$, 1 $CaCl_2$, 10 glucose and 10 HEPES adjusted to pH 7.4. The pipette solution (intracellular solution) was composed of (in mmol/L): 140 KCl, 1 $MgCl_2$, 2 EGTA, 1.71 $CaCl_2$ (1 μM $[Ca^{2+}]$ free) and 5 HEPES (adjusted to pH 7.2 with KOH). The concentration of Ca^{2+} in the pipette solution was present to activate Ca^{2+-}activated K^+ (KCa) currents. Recordings were digitized on line using a Digidata 1440A (Axon Instruments) and to acquire and store data pClamp 10 software was used. Current-voltage relationships were constructed using voltage ramps (-100 to 100 mV, 500 msec) at a holding potential (Vh) of −50 mV. Amplitude of K^+ currents were normalized to cell capacitance (pA/pF) to account for differences in current density. ACh (10 μmol/L) and blockers of $K_{Ca}3.1$ and $K_{Ca}2.3$ channels, TRAM-34 (1 μmol/L) and UCL 1684 (1 μmol/L), respectively, were applied to the recording μ-dish via a gravity-fed U-tube microperfusion system connected to a vacuum pump.

2.8. Western blot analysis

The protein levels of CYP2C11, CYP2C23 and CYP4A enzymes were assessed in rat interlobar arteries and renal cortex fractions from LZR and OZR rats by Western blot as earlier reported [22]. Briefly, samples were homogenized on ice in lyses buffer (10 mM Tris-HCl (pH 7.4), 1% SDS, 1 mM sodium vanadate and 0.01% protease inhibitor cocktail (Sigma Aldrich, Madrid, Spain) and after centrifugation (15,000*g* for 20 min at 4 °C), proteins were quantified by the DC Protein Assay Kit (Bio-Rad Madrid Spain). For each sample 65-90 μg, protein was boiled in Laemmli sample buffer and loaded into each well of a were separated in 10% polyacrylamide gels (SDS-PAGE) and, after migration, were transferred to a polyvinylidene fluoride (PVDF) membranes (GE Healthcare, Madrid, Spain) for 70 min at 35 V (Bio-Rad, Madrid, Spain). All membranes were blocked in 5% non-fat dry milk for 1 h at room temperature and then incubated overnight at 4 °C with the following rabbit polyclonal primary antibodies: anti-CYP2C11 (1/300) anti-CYP2C23 (1/300) and anti-CYP4A (1/150) (Abcam, Bristol, UK). After washing in 0.05% Tween-20, membranes were incubated with HRP-conjugated secondary antibodies for 1 h at room temperature, and then washed and visualized by chemiluminescence (ECL advance-kit, GE Healthcare, Madrid, Spain) using anti-β-actin antibody (Santa Cruz Biotechnology, Quimigen, Madrid, Spain) as loading control. Quantification of protein levels was made using Image Quant 5.0 software (GE Healthcare Life Sciences) and expressed as densitometry units relative to loading control.

2.9. Immunohistochemistry

Immunohistochemical analysis was conducted to substantiate the western blot findings and also to localize the changes in CYP2C23, CYP2C11 and CYP4A in kidney sections of preglomerular arteries and renal cortex [22,25]. Paraffin-embedded tissue slides (4 μm) from kidney were de-waxed and antigen retrieval was carried out in 10 mM citrate buffer, pH 6.0 and blocked for 10 min with 0.3% hydrogen peroxide at room temperature. Tissues were blocked in 5% donkey serum and incubated overnight at 4 °C with the following biotinylated primary antibodies: anti-CYP2C11 (1/50) anti-CYP2C23 (1/50) and

anti-CYP4A (1/50) (Abcam, Bristol, UK). After washes, sections were covered with the appropriated biotinylated secondary antibody. Washed sections were then incubated with streptavidin–biotin conjugated horseradish peroxidase (HRP) (EMD Millipore Corp., Darmstadt, Germany) for 30 min followed by incubation with 3, 3′-diaminobenzidine (DAB) (Sigma Aldrich, Madrid, Spain) for color development. The sections were counterstained by Harris's hematoxylin, dehydrated and mounted.

K_{Ca} channel expression in the arterial wall of preglomerular arteries was determined by immunofluorescence by incubating renal sections from LZR and OZR with primary antibodies anti-small conductance K_{Ca} ($K_{Ca}2.3$) channel (Alomone, Israel, 1:200 dilution) or anti-intermediate conductance K_{Ca} ($K_{Ca}3.1$) channel (Alomone, Israel, 1:450 dilution) along with a mouse monoclonal anti-eNOS (Abcam, Cambridge, UK) diluted at 1:400 for 48 h, washed and allowed to react with a secondary antibody, Alexa Fluor 594 (red) goat-antirabbit (Invitrogen, Life Technologies S.A., Spain, 1:200 dilution) and Alexa Fluor 488 (green) goat-antimouse (Invitrogen, UK, 1:200 dilution). Slides were finally

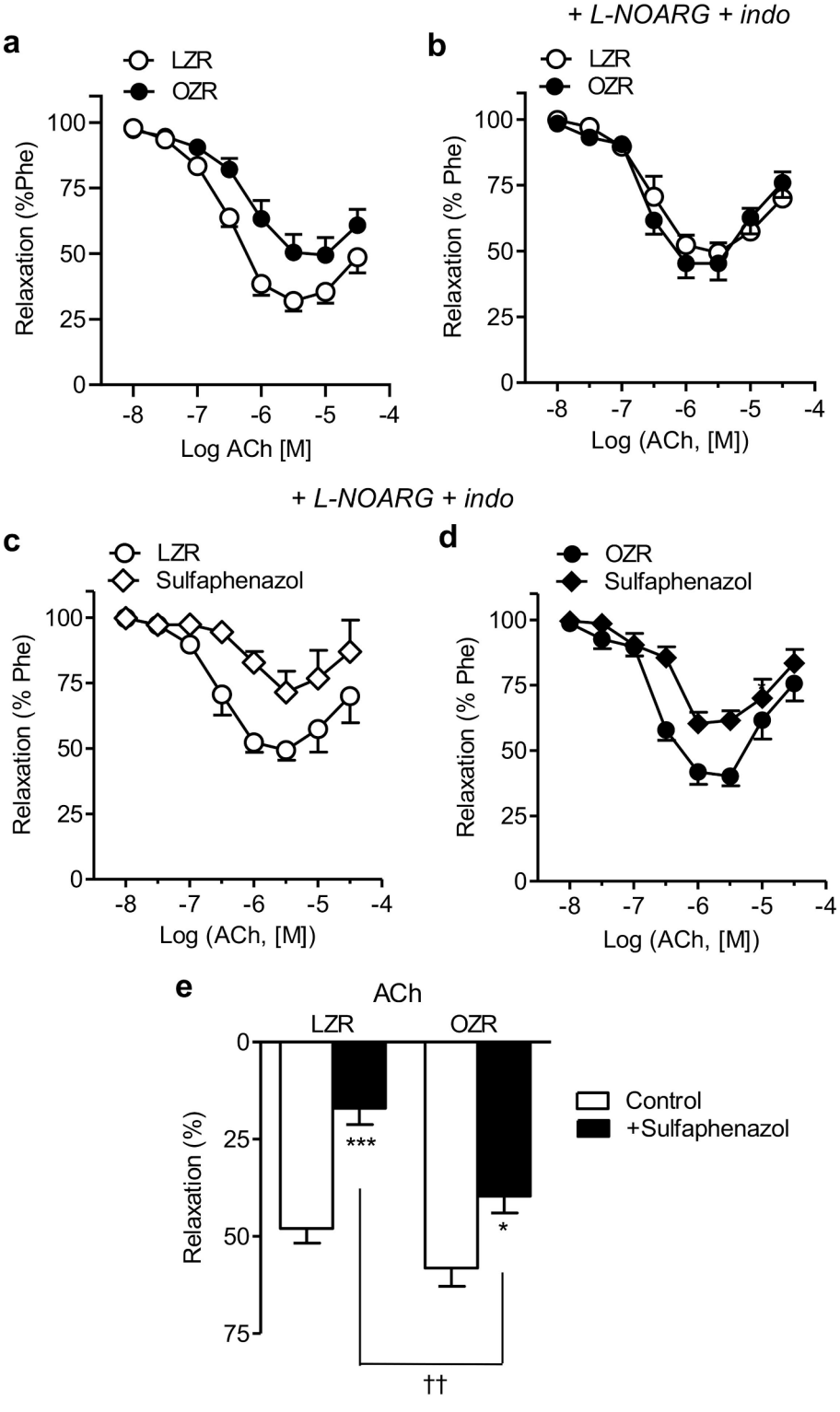

Fig. 1. Impaired CYP2C-mediated vasorelaxation in kidney preglomerular arteries of OZR. (a,b) Average relaxations to ACh in the absence (a) and presence (b) of NOS and COX blockers, L-NOARG (100 μM) and indomethacin (0.3 μM), respectively, in renal interlobar arteries from OZR compared to LZR. (c-e) Effect of the CYP2C inhibitor sulfaphenazole (1 μM) on the average concentration-dependent (c,d) or maximal (e) relaxant responses to ACh in renal arteries from LZR and OZR. Results are expressed as percent of the precontraction induced by phenylephrine (Phe). Data are shown as the mean ± SEM of 7–9 arteries of 5 rats *$p < 0.05$, **$p < 0.01$, ***$p < 0.001$, *versus* control before treatment, ††$p < 0.01$, *versus* LZR, Students *t*-test for paired or unpaired observations.

covered with a medium containing DAPI for cell nuclei staining. Observations were made with a fluorescence microscope (Olympus IX51). No immunoreactivity could be detected in sections incubated without the primary antisera. Preadsorption with K_{Ca} channel proteins showed no cross-reactivity to the antibodies.

2.10. Data presentation and statistical analysis

Results are expressed as a percent of the responses to Phe, as means ± SEM of 5–9 arteries (1–2 from each animal) for the functional assays. Results are expressed in counts per minute (cpm) or relative fluorescence units (RFU) per mg of tissue for measurements of $O_2^{\bullet-}$ or H_2O_2, respectively, in arterial segments and cortex samples, as means ± SEM of 5–13 animals. Results of Western Blotting analysis were quantified by densitometry units and expressed relative to the β-actin content in arteries or cortex samples, as means ± SEM of 4–5 animals. For electrophysiology, experiments were measured as a relationship between amplitudes of K^+ currents and maximal amplitude in control condition, as means ± SEM of 6a arteries (1 from each animal). Statistical differences between means were analyzed by paired or unpaired Student́s *t*-test for comparison between two groups, or by one-way ANOVA followed by Bonferroní*s post hoc* test for comparisons involving more than two groups. Probability levels lower than 5% were considered significant. All calculations were made using the software package Prism 8.0 (GraphPad, San Diego, CA).

3. Results

3.1. Impaired CYP2C epoxygenase-mediated endothelium-dependent relaxations and H_2O_2 production in renal preglomerular arteries of OZR

Endothelial function was assessed by the relaxations to ACh in interlobar arteries of LZR and OZR. In arteries precontracted with Phe, Ach-induced dose-dependent relaxations were impaired in arteries from OZR compared to LZR (Fig. 1**a**), while under conditions of NOS and COX enzymes blockade these relaxations were unchanged or even enhanced (Fig. 1**b**). However, the inhibitory effect of the CYP2C inhibitor sulfaphenazole on the relaxations induced by ACh was significantly reduced in renal arteries from obese rats compared to that in control rats (Fig. 1**c, d,e)**, suggesting an impaired participation of CYP2C epoxygenase in these EDH-type relaxations.

The contribution of CYP epoxygenases to NADPH-dependent ROS generation and oxidative stress in obese rats was further assessed. NADPH-stimulated $O_2^{\bullet-}$ generation was augmented in both arteries and renal cortex of OZR and inhibited by sulfaphenazole **(**Fig. 2**a,b**). In contrast, NADPH-derived H_2O_2 levels were significantly reduced in interlobar arteries of obese rats compared with lean controls and they were no longer inhibited by sulfaphenazole (Fig. 2**c**) thus suggesting an impaired CYP2C-mediated H_2O_2 production in renal preglomerular arteries of OZR. Both basal and NADPH-derived H_2O_2 were reduced in renal cortex samples of OZR, and sulfaphenazole did not significantly inhibit NADPH-derived H_2O_2 in renal cortex samples from either LZR or OZR (Fig. 2**d**)

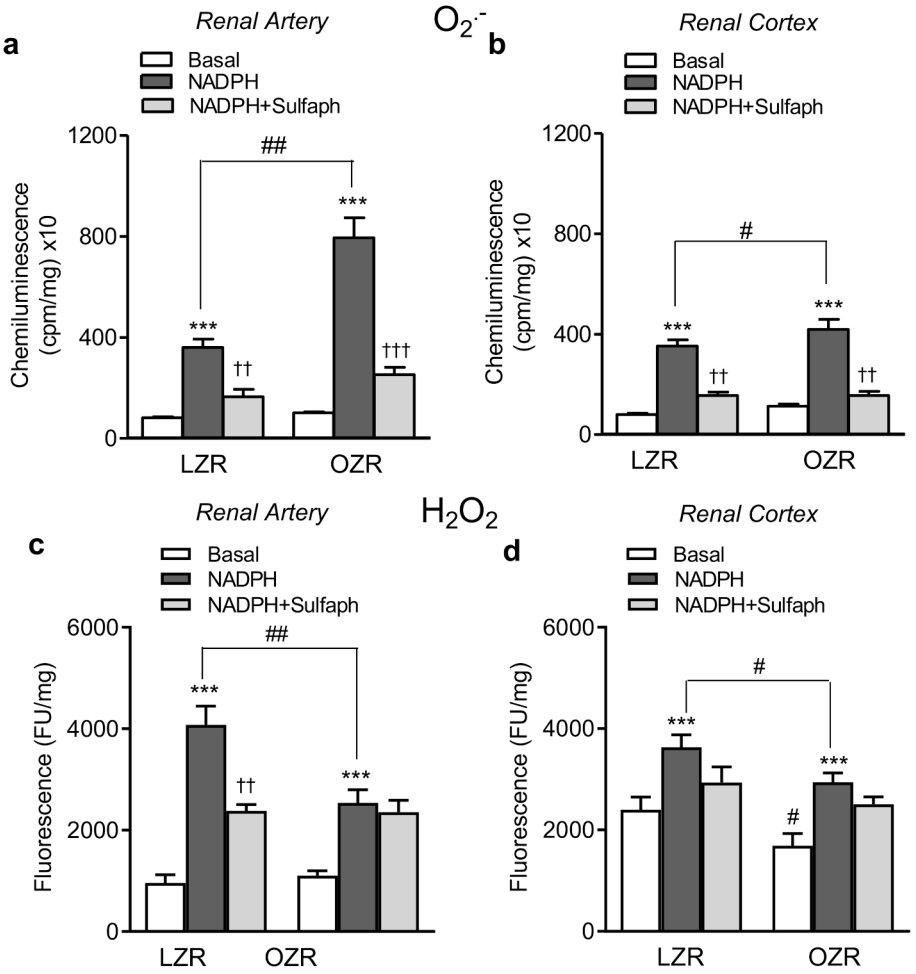

Fig. 2. Impaired CYP2C-mediated H_2O_2 production in kidney preglomerular arteries of OZR (**a-d**) Basal and NADPH-stimulated $O_2^{\bullet-}$ and H_2O_2 production and effect of the CYP2C inhibitor sulfaphenazole (1 μM) on renal interlobar arteries and cortex from LZR and OZR, measured by (**a,b**) lucigenin-enhanced chemiluminiscence and (**c,d**) Amplex Red fluorescence assays, respectively, in renal artery (a,c) and renal cortex (b,d). Results are expressed as counts per minute (cpm) or relative fluorescence units (RFU) per mg of tissue, for chemiluminescence or Amplex Red assay, respectively. Bars represent mean ± SEM of 5–13 animals. Statistically significant differences were calculated by unpaired Student's *t*-test or ANOVA followed by Bonferroni posterio test. ***p < 0.001 *versus* basal levels, ††p < 0.01 †††p < 0.001 *versus* NADPH-stimulated; #p < 0.05; ##p < 0.01 *versus* LZR.

3.2. Downregulation of CPY2C11 and CPY2C23 in renal interlobar arteries of OZR

Distribution and levels of CYP2C epoxygenases were further assessed in kidney vascular and cortical samples of LZR and OZR. Both CYP2C11 (Fig. 3**a, c**) and CYP2C23 (Fig. 3**b, d**) proteins were decreased in interlobar arteries of OZR compared with lean controls. Immunoreactivity for CYP epoxygenases was found in vascular smooth muscle (VSM) and endothelial layer of renal arteries from both LZR and OZR, but intensity of immunostaining was lower in arteries but not renal cortex of OZR compared to LZR (Fig. 3**a and b**). Western blot analysis confirmed these findings and showed a reduced expression of both enzymes in OZR compared to LZR (CYP2C11, 28% ($p < 0.01$) (Fig. 3**c**); CYP2C23, 22% ($p < 0.01$) (Fig. 3**d**)). Obesity thus seems to down-regulate CYP2C11 and CYP2C23 proteins in intrarenal arteries but not in renal cortex wherein CYP2C23 and CYP2C11 protein levels and immunoreactivities were similar in LZR and OZR (Fig. 3**a-d**).

3.3. Enhanced expression and activity of $K_{Ca}3.1$ and $K_{Ca}2.3$ channels preserve endothelium-dependent relaxations of renal interlobar arteries of OZR

The compensatory mechanisms preserving EDH-type endothelium-dependent relaxations in interlobar arteries of OZR were further investigated. Increasing concentrations of ACh elicited relaxations that were accompanied by simultaneous decreases in VSM $[Ca^{2+}]_i$, indicating that EDH-type vasorelaxation is preserved in obese compared to control animals (Fig. 4**a,b**). Expression and distribution of K_{Ca} channels in the arterial wall was assessed by immunofluorescence in renal preglomerular arteries from LZR and OZR. Immunostaining of arterial sections with anti-$K_{Ca}3.1$ and anti-$K_{Ca}2.3$ antibodies revealed that these channels were uniformly distributed and colocalized with eNOS at the endothelial lining, being absent in the VSM layer in arteries from LZR (Fig. 4**c**). Interestingly, endothelial expression of both K_{Ca} channels was significantly augmented in preglomerular arteries from obese rats, and immunostaining for $K_{Ca}3.1$ was even spread to and detected in VSM (Fig. 4**c**).

The contribution of these K_{Ca} channels to the ACh-induced endothelial relaxation of renal arteries of LZR and OZR was elucidated by testing the effects of specific blockers on the responses to ACh under conditions COX and NOX inhibition. Combined treatment with TRAM-34 (1 μM) and UCL 1684 (1 μM) markedly reduced ACh-induced relaxations in LZR (Fig. 4**d**) and abolished those in OZR (Fig. 4**e**). The contribution of $K_{Ca}3.1$ and $K_{Ca}2.3$ channels to the ACh-induced currents in RIAECs was further evaluated in 'whole-cell' patch-clamp experiments performed in freshly isolated native endothelial cells (ECs) from intrarenal arteries. In single cells, a voltage-ramp from − 100 to + 100 mV, 600 ms (Vh = − 50 mV) and 1 μM Ca^{2+} into the patch-pipette activated K^+ outward currents that were voltage-dependent and showed outward rectification at the more positive membrane potentials which corresponded to the basic electrophysiological properties of $K_{Ca}1.1$ channels (not shown). Addition of 10 μM ACh to the perfusate increased baseline current and further application of a voltage-ramp significantly enhanced the amplitude and induced a change in the

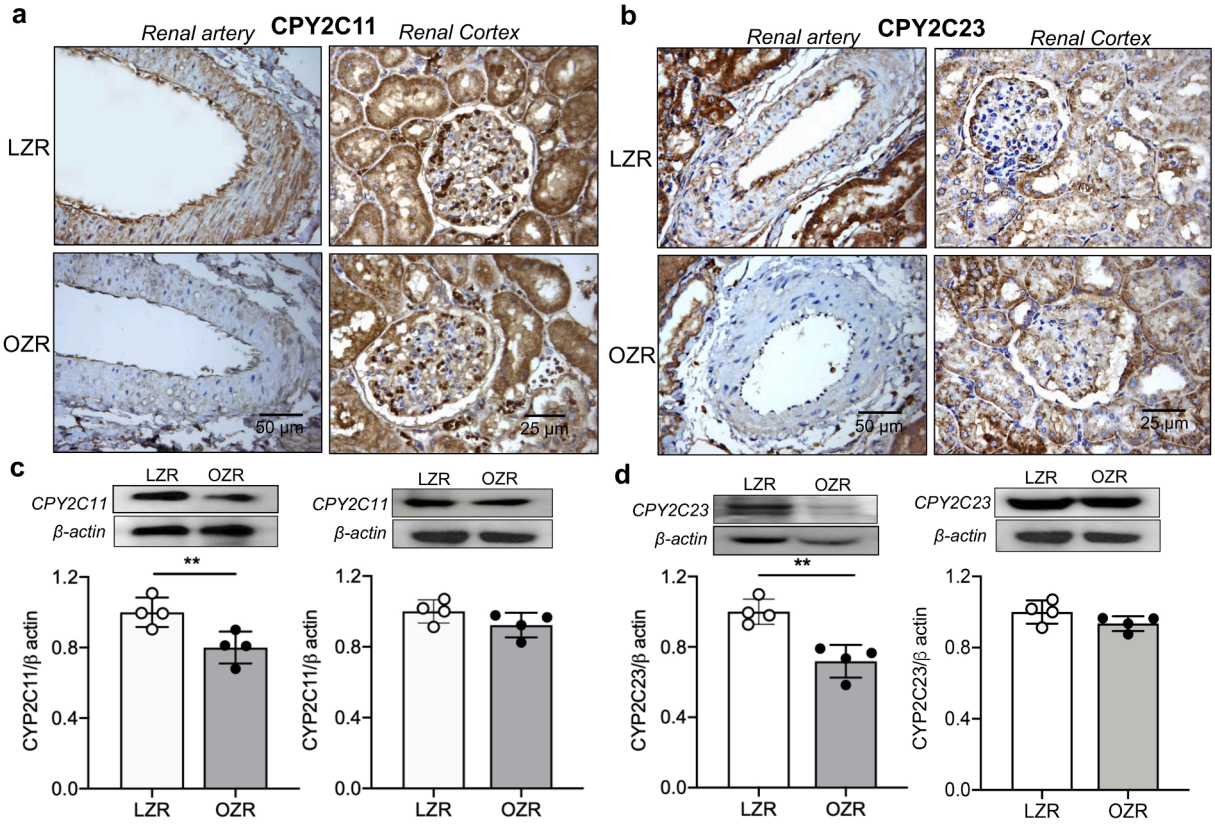

Fig. 3. Downregulation of CYP2C enzymes in preglomerular arteries of obese rats. (**a,b**) Inmunohistochemical demonstration of CYP2C11 (a) and CYP2C23 (b) in renal interlobar artery (left column) and renal cortex (right column) from rat kidney of LZR and OZR. CYP2C protein was distributed throughout the arterial wall at both endothelium and VSM in arteries and arterioles, with a lower density of both CYP2C11 (**a**) and CYP2C23 (**b**) in arteries of obese rats. CYP2C11 and CYP2C23 immunoreactivity was also present in renal cortex samples (renal tubules and glomeruli) with no differences in density between LZR and OZR. Sections are representative of n = 3 animals. (**c,d**) Western blot analysis of CYP2C11 and CYP2C23 expression in samples of renal artery and cortex showing that CYP2C11 (c) and CYP2C23 (d) protein levels were lower in renal arteries but unchanged in renal cortex of OZR compared to LZR. Results were quantified by densitometry and presented as a ratio of density of CYP2C11 and CYP2C23 bands *vs* those of β-actin from the sample. Data are expressed as the mean ± SEM of 4–5 animals. Significant differences were analyzed using unpaired *t*-test *$p < 0.05$; **$p < 0.01$ versus LZR.

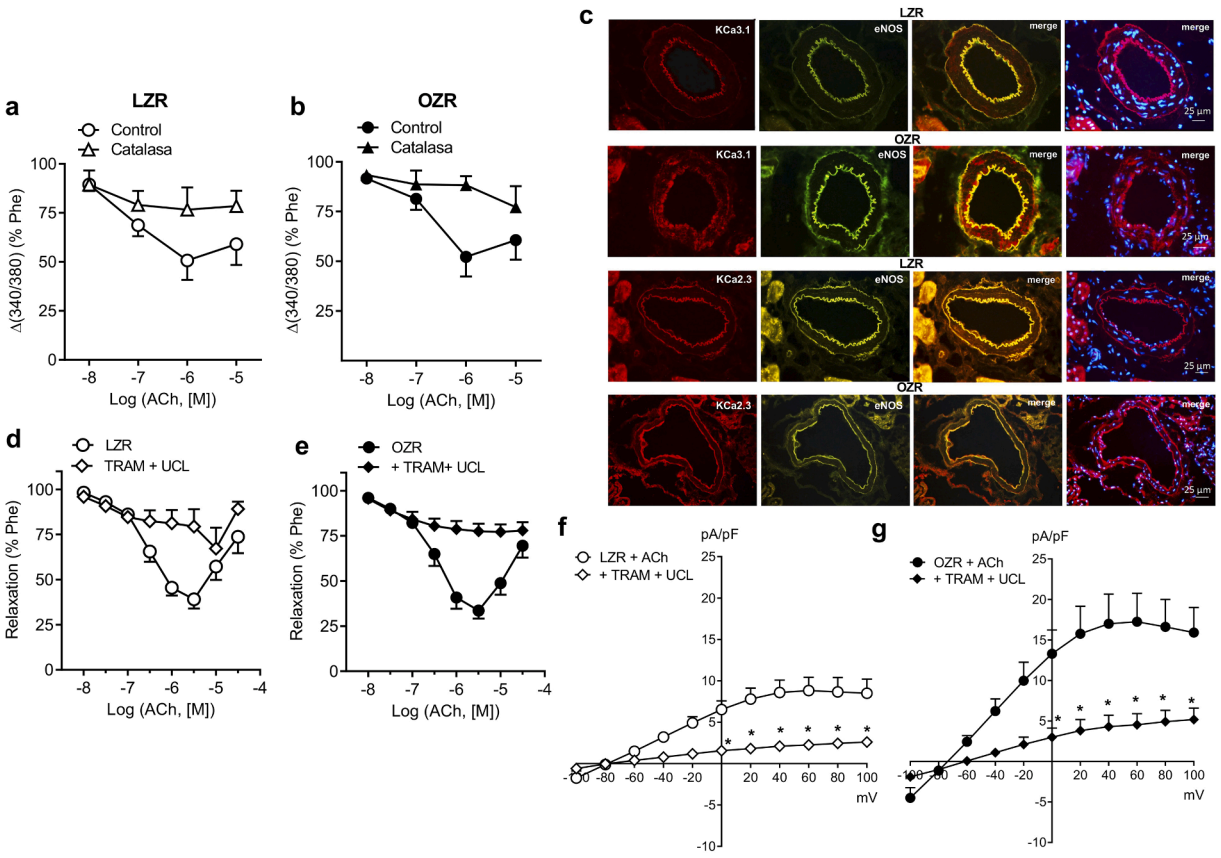

Fig. 4. Preserved EDH-type vasorelaxation and enhanced K_{Ca} channels activity in renal interlobar arteries of OZR. (a,b) Average concentration-dependent decreases in $[Ca^{2+}]_i$ and inhibitory effect of catalase in renal interlobar arteries of (a) LZR and (b) OZR. (c) Immunofluorescence for $K_{Ca}3.1$ and $K_{Ca}2.3$ proteins was distributed throughout the endothelial lining in arteries of LZR and OZR (red areas) and was markedly increased in OZR wherein immunostaining extended also to VSM in the case of $K_{Ca}3.1$ channels. Endothelial cell layer was visualized with the anti-eNOS marker (green). Sections are representative of n = 3 animals. (d,e) Inhibitory effect of $K_{Ca}3.1$ and $K_{Ca}2.3$ channel blockers TRAM-34 (1 μmol/L) and UCL 1684 (1 μmol/L), respectively, on the relaxations induced by ACh under conditions of NOS and COX blockade in renal interlobar arteries of (d) LZR and (e) OZR. Data are shown as the mean ± SEM of 5–7 arteries of 5 animals. **(f)** Average I-V relationships for K^+ currents in isolated RIAECs from LZR and OZR evoked by voltage-ramps from −100 to + 100 mV, 500 msec, Vh = -50 mV, in the presence of ACh (10 μmol/L) and after the addition of TRAM-34 (1 μmol/L) plus UCL 1684 (1 μmol/L), blockers of $K_{Ca}3.1$ and $K_{Ca}2.3$ channels, respectively. Results are expressed as current amplitude normalized to current density (pA/pF) Data are mean ± SEM of n = 6–8 animals. *p < 0.05 using two-way ANOVA with Bonferroni post-test.

shape of the outward currents corresponding to $K_{Ca}3.1$ and $K_{Ca}2.3$ currents in RIAECs (Fig. 4**f**,**g**). These effects of ACh were significantly increased in RIAECs of OZR (Fig. 4**g**) compared to LZR (Fig. 4**f**). Combined blockade of both $K_{Ca}3.1$ channels with TRAM-34 (1 μM) and the $K_{Ca}2.3$ with UCL 1684 (1 μM) significantly inhibited both the ACh-induced resting outward current, the outwardly directed and voltage-independent currents, as well as the inward current at the more negative potentials (Fig. 4**f**,**g**), inhibition being larger in obese compared to control animals. These results suggest that enhanced functional expression of $K_{Ca}3.1$ and $K_{Ca}2.3$ channels contributes to EDH-type relaxations of preglomerular OZR arteries and thus compensates for impaired endothelium-dependent relaxations.

3.4. Up-regulation of CPY4A is associated with enhanced Nox-dependent $O_2^{\bullet-}$ production and impaired endothelial NO-mediated relaxations in renal interlobar arteries of OZR

Immunohistochemistry, Western blots and densitometric analysis of CYP4A protein in the interlobar arteries and renal cortex of Zucker rats are shown in Fig. 5. CYP4A immunoreactivity was low in interlobar arteries of LZR but significantly increased in OZR showing a stronger signal compared with that of LZR in both VSM and the endothelial layer of renal interlobar arteries (Fig. 5a). Western Blot confirmed a markedly enhanced CYP4A expression that increased by 28% ($p < 0.05$) in OZR rats compared to LZR (Fig. 5b). This result suggests that obesity significantly upregulated CYP4A enzyme in isolated renal arteries. However, no significant differences were found in the content of CYP4A protein when comparing renal cortex of LZR and OZR (Fig. 5**c**). CYP4A immunoreactivity revealed a similar localization and intensity in tubules, glomeruli and endothelial lining of arterioles in renal cortex samples of obese animals compared to controls (Fig. 5**a**).

The effect of the selective inhibitor of CYP4A hydroxylase mediated-20-HETE biosynthesis HET-0016, and the NADPH oxidase inhibitor apocynin were examined on ROS production of intrarenal arteries. Both treatments reduced to a similar extent $O_2^{\bullet-}$ formation stimulated by NADPH in LZR and OZR (Fig. 6a). Both HET-0016 and apocynin had a larger inhibitory effect on $O_2^{\bullet-}$ production in OZR (Fig. 6**a**), wherein $O_2^{\bullet-}$ generation was augmented compared to control rats (Fig. 6**a**). To determine whether changes in CYP4A metabolism may be involved in the endothelial dysfunction of OZR preglomerular arteries, the effect of HET-0016 was assessed on the endothelium-dependent relaxations elicited by ACh in the absence of NOS blockade, these relaxations being significantly enhanced by HET-0016 in arteries from OZR (Fig. 6**c**) without altering those from LZR (Fig. 6**a**). These results confirm the involvement of CYP4A -derived ROS in the impaired NO-mediated relaxations of obese rats preglomerular arteries.

4. Discussion

Oxidative stress derived from Nox, COX-2 and xanthin oxidase is

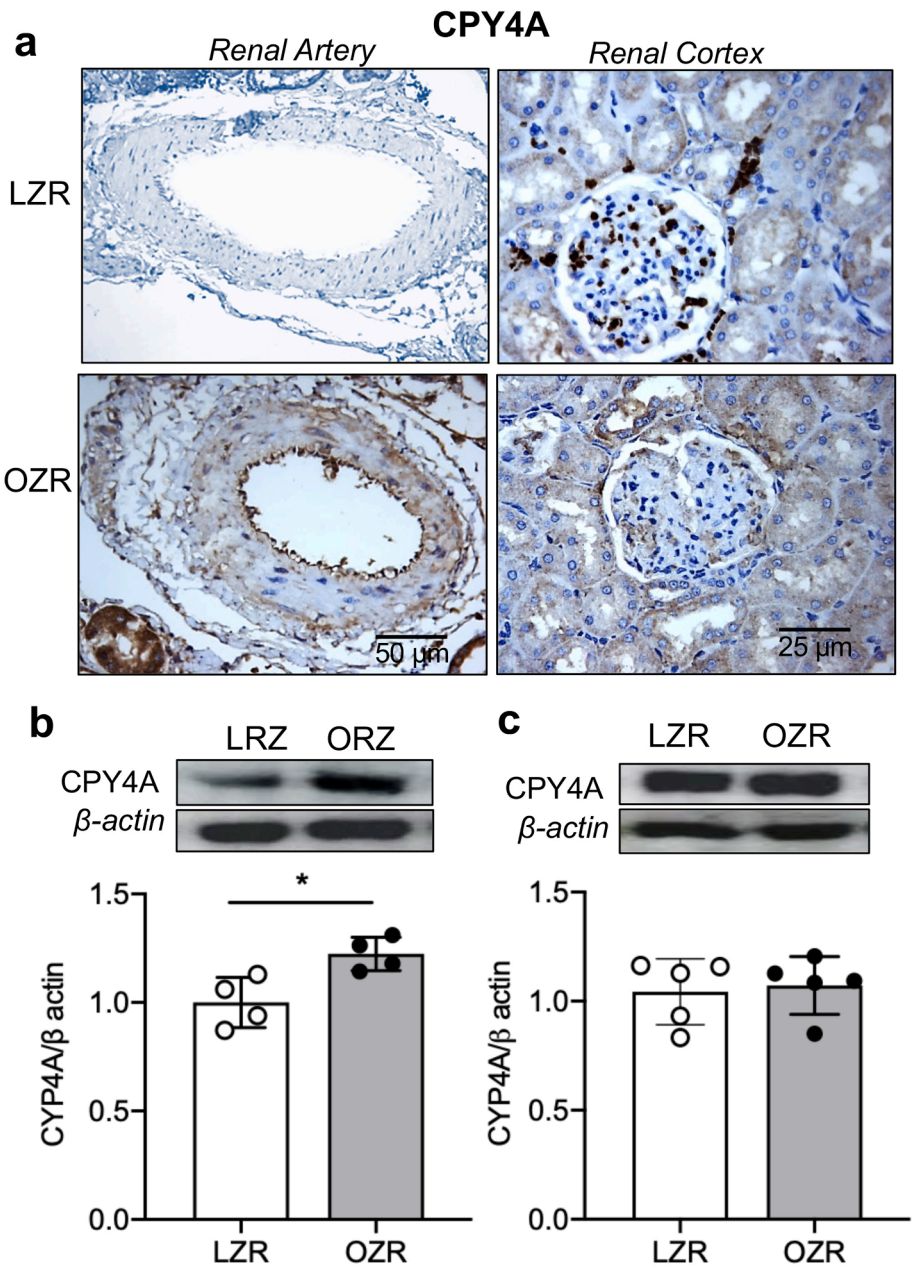

Fig. 5. Upregulation of CPY4A in renal preglomerular arteries of OZR. Representative immunoreactivity and Western blots and densitometric analysis of CYP4A protein in interlobar arteries and renal cortex of Zucker rats. (**a**) CYP4A protein was distributed throughout the endothelial lining and also in VSM of the renal interlobar arteries, with a higher density in OZR compared to LZR. CYP4A immunoreactivity was also present in renal cortex samples (renal tubules and glomeruli) with no differences in density between LZR and OZR. Sections are representative of n = 3 animals. (**b,c**) Western blot analysis of CYP4A expression in samples of renal artery and cortex of LZR and OZR kidney showing that CYP4A protein levels were lower in interlobar arteries from LZR than in those of OZR, with no differences in renal cortex samples from both animals. Results were quantified by densitometry and presented as the ratio of CYP4A band density *vs* that of β-actin in the sample. Data are shown as the mean ± SEM of 4–5 animals. Significant differences were analyzed using unpaired *t*-test *$p < 0.05$ versus LZR.

involved in kidney endothelial dysfunction in obesity and insulin-resistant states [14,20,21,22]. We demonstrate here that CYP enzymes differentially contribute to oxidative stress and impaired endothelial function of kidney preglomerular arteries from obese rats; whereas CYP4A upregulation and augmented ROS generation underlie impaired NO-mediated relaxations, downregulation of CYP2C11 and CYP2C23 was associated to reduced CYP2C-derived levels of vasodilator H_2O_2 in obese rats which was compensated by enhanced functional expression of $K_{Ca}3.1$ and $K_{Ca}2.3$ channels.

Decreased expression and activity of CYP2C epoxygenases and impaired vasodilation and albuminuria was earlier reported in renal afferent arterioles during the onset of obesity-related hypertension and type 2 diabetes [14,16]. In mesenteric microvessels from obese rats, endothelial dysfunction related to downregulation of CYP2C11 activity was ascribed to impaired EDH-type relaxations [15]. In renal preglomerular arteries, vasodilator H_2O_2 is generated as a by-pass product of endothelial CYP epoxygenase activity and participates in the EDH vasodilator responses, while CYP2C-derived EETs seem to have a major vasoconstrictor role and counterbalance endothelium-dependent H_2O_2-mediated relaxations, as depicted by the inhibitory effect of sEH on EDH-type relaxations [9]. The present data confirm that CYP2C11 and CYP2C23 are down-regulated in kidney preglomerular arteries from obese rats, as earlier reported in glomeruli and renal microvessels [14], and further demonstrate that decreased expression of endothelial CYP2C epoxygenases is associated with a reduced generation of vascular H_2O_2 and with a lesser sensitivity of EDH-dependent relaxations to the CYP2C inhibitor sulfaphenazole. Nevertheless, despite blunted arterial levels of CYP2C-derived vasodilator H_2O_2, EDH-type renal endothelial relaxations were preserved in obese rats compared to those in lean controls and maintained by up-regulation and enhanced activity of endothelial $K_{Ca}3.1$ channels. $K_{Ca}3.1$ and $K_{Ca}2.3$ channels are functionally expressed at the renal endothelium and play a key role in the EDH-mediated relaxations of kidney preglomerular arteries [26]. CYP epoxygenase-derived H_2O_2 enhances endothelial $K_{Ca}3.1$ currents and the subsequent hyperpolarization spreads to VSM to reduce $[Ca^{2+}]_i$ and to evoke EDH-type vasodilatation [9]. In the present study, H_2O_2-

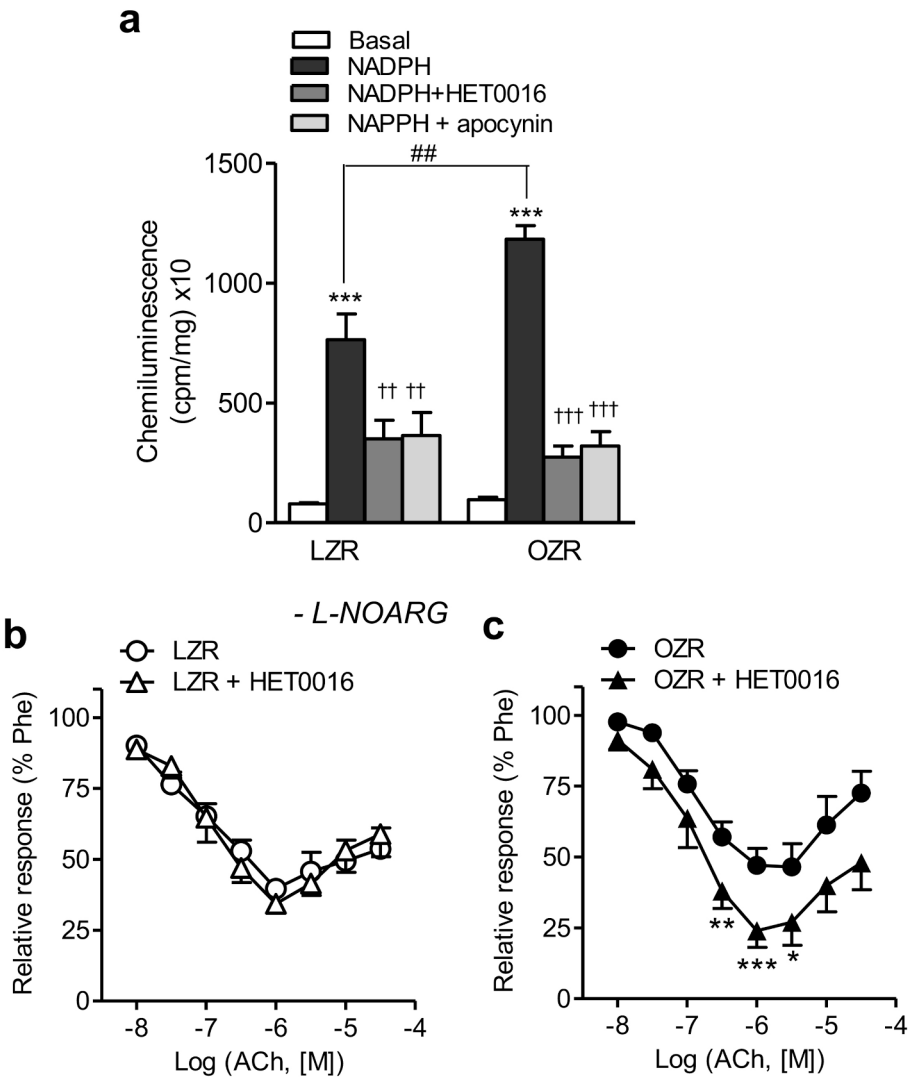

Fig. 6. CYP4A is involved in the enhanced Nox-dependent $O_2^{\bullet-}$ production and impaired NO-mediated relaxation of preglomerular arteries of OZR. (**a**) Effects of the selective inhibitor of CYP450-mediated 20-HETE biosynthesis HET0016 and of the Nox inhibitor apocynin on the NADPH-stimulated levels of $O_2^{\bullet-}$ measured by lucigenin-enhanced chemiluminescence in renal arteries of LZR and OZR. Results are expressed in counts per minute (cpm) per mg of tissue. Bars represent mean ± SEM of 7 animals. Statistical significance was determined by one-way ANOVA followed by Bonferroni as *a posterio test* ***p < 0.001 versus basal levels, ††p < 0.01; †††P < 0.001 versus NADPH-stimulated, ##p < 0.01 versus LZR. (**b,c**) Average inhibitory effect of the inhibitor of the CYP4A-mediated 20-HETE biosynthesis HET-0016 on the relaxations induced by the endothelial agonist ACh in renal arteries of (**b**) LZR and (**c**) OZR. Data are shown as the mean ± SEM of 6–7 arteries of 5 animals. Statistical significance was determined by Student *t*-test for paired observations *p < 0.05; **p < 0.01; ***p < 0.001 versus control before treatment.

mediated ACh-induced decreases in VSM $[Ca^{2+}]_i$ were similar in preglomerular arteries from LZR and OZR and coupled to preserved non-NO non-prostanoid EDH type relaxations in OZR. These relaxations were abolished by blockade of $K_{Ca}3.1$ and $K_{Ca}2.3$ channels. Moreover, endothelial $K_{Ca}2.3$ channels were found to be up-regulated whereas $K_{Ca}3.1$ channel expression was greatly enhanced not only at the endothelium but also spread to the adjacent VSM, as earlier reported by our group in coronary arteries of genetically obese rats, wherein enhanced K_{Ca} channel-mediated relaxations contributed to preserve coronary endothelium-dependent relaxations involving NO [28]. We further first demonstrate here that up-regulation of renal endothelial K_{Ca} channels is associated with enhanced endothelial $K_{Ca}3.1$ and $K_{Ca}2.3$ currents, this mechanism being responsible for the increased EDH-type responses that compensate for impaired NO-mediated vasodilation in preglomerular arteries from obese/insulin resistant rats. Preservation of endothelial function involving EDH-relaxations has earlier been proposed for small arteries from type II diabetic patients [29] and diabetic rats [30].

CYP4A-derived 20-HETE levels are elevated in resistance arteries from hypertensive animal models and its role in the development of hypertension is well established [18,31–34]. Obesity and HFD markedly enhance expression of CYP4A/F genes, through activation of PPARα in animals and inhibition of HNF4α in humans [35], elevated blood and urine levels of 20-HETE being correlated with body mass index (BMI) in humans [36,37]. Increased 20-HETE levels in HFD models contribute to both metabolic and cardiovascular complications of metabolic syndrome and are involved in the impaired insulin signaling leading to insulin resistance [17] and in the pathogenesis of hypertension [18,19,38,39]. In the present study, increased expression of CYP4A protein at both endothelium and VSM was associated to endothelial dysfunction in preglomerular arteries from obese rats, as shown by the reversal of the impaired NO-mediated relaxations by the inhibitor of 20-HETE biosynthesis HET0016 in arteries from OZR. These findings are in agreement with those earlier reported for intracerebral arteries of hypertensive [40] and for coronary arteries of metabolic syndrome [19] rats, wherein inhibitors of 20-HETE synthesis ameliorated endothelial dysfunction both *in vivo* and *in vitro*. In patients with coronary artery disease (CAD), individuals with the highest plasma levels of 20-HETE were susceptible to more advanced endothelial dysfunction, measured as brachial artery flow-mediated dilatation [41].

20-HETE has been reported to impair endothelial function through uncoupling of eNOS or impairment of eNOS Ser1179 phosphorylation [19,32,42,43], oxidative stress and activation of the NF-κB pro-inflammatory signaling pathways underlying 20-HETE-associated endothelial dysfunction [42–47]. Clinical studies have also confirmed a correlation between urinary or plasma 20-HETE levels, oxidative stress and endothelial dysfunction in humans [48,49]. Our data demonstrate that Nox-derived enhanced $O_2^{\bullet-}$ production is involved in endothelial dysfunction associated to upregulation of CYP4A in intact preglomerular arteries of insulin-resistant obese rats, since augmented NADPH-derived $O_2^{\bullet-}$ levels were markedly reduced by both the 20-HETE synthesis

inhibitor HET0016 and by the Nox inhibitor apocynin. 20-HETE activates Nox2 in bovine pulmonary artery and aorta endothelial cells by promoting translocation and tyrosine phosphorylation of p47phox and activation of Rac1/2 [45]. Both Nox1 and Nox2 contribute to vascular oxidative stress and endothelial dysfunction in intrarenal arteries of obese rats [22] and therefore, the present data suggest that upregulation of CYP4A and increased 20-HETE levels are involved in Nox-derived arterial oxidative stress and endothelial dysfunction of insulin-resistant obese Zucker rats. Augmented CYP4A-derived 20-HETE production has also been reported to contribute to enhanced Nox1 and Nox4 expression and $O_2^{\bullet-}$ production in glomeruli, and to podocyte injury and apoptosis in type 1 diabetic mice; albuminuria and podocyte injury were ameliorated by in vivo treatment with HET0016 in these animals [50]. In the kidney, overexpression of CYP4A2 resulted in increased 20-HETE levels, impaired Akt/eNOS/NO endothelial pathway, enhanced $O_2^{\bullet-}$ production, renal injury and hypertension [30]. In the present study we found that obesity-induced enhanced expression of CYP4A was restricted to vascular tissues while no significant changes in CYP4A protein content and expression were observed in renal tubules from kidney cortex samples of OZR. Therefore, arterial oxidative stress and endothelial dysfunction associated to CYP4A upregulation of preglomerular arteries might contribute to hypertension and further progression to renal damage and albuminuria in these prediabetic prehypertensive obese Zucker rats [14,51].

In conclusion, the current data demonstrate that both decreased endothelial CYP2C11/ CYP2C23-derived vasodilator H_2O_2 and augmented CYP4A-derived 20-HETE contribute to endothelial dysfunction and vascular oxidative stress in prehypertensive prediabetic obese-insulin resistant rats. While compensatory upregulation of $K_{Ca}3.1$ and $K_{Ca}2.3$ channels preserves EDH-type vasodilation in prediabetic stages, CYP4A inhibitors ameliorate arterial oxidative stress and restore endothelial function which suggests that CYP4A-derived 20-HETE may be involved in the pathogenesis of hypertension and albuminuria and supports the therapeutic potential of 20-HETE inhibitors for the vascular complications of obesity-associated kidney injury.

Declaration of Competing Interest

The authors declare that they have no known competing financial interests or personal relationships that could have appeared to influence the work reported in this paper.

Acknowledgements

This work was supported by PID2019-105689RB-I00 (Ministerio de Ciencia e Innovación, Spain) cofounded by the FEDER Program of EU, and grant for UCM research group from Universidad Complutense de Madrid. Manuel Perales and Francisco Puente are thanked for expert technical assistance.

Author contributions

D.P conceived the idea and designed the study. M.M., E.LO, C.R., E.P, M.P.M. and AG conducted the experiments and analyzed data; M.M., E. LO, L.R. and D.P wrote the manuscript; C.C., S.B. and J.S-M. contributed to the Discussion; D.P. and L.R. revised the final manuscript.

References

[1] J.D. Imig, Epoxyeicosatrienoic acids, 20-hydroxyeicosatetraenoic acid, and renal microvascular function, Prostagl. Other Lipid Mediat. 104–105 (2013) 2–7.
[2] F. Fan, R.J. Roman, Effect of cytochrome P450 metabolites of arachidonic acid in nephrology, J. Am. Soc. Nephrol. 28 (10) (2017) 2845–2855.
[3] Y. Deng, K.N. Theken, C.R. Lee, Lee CR cytochrome P450 epoxygenases, soluble epoxide hydrolase and the regulation of cardiovascular inflammation, J. Mol. Cell. Cardiol. 48 (2) (2010) 331–341.
[4] W.B. Campbell, I. Fleming, Epoxyeicosatrienoic acids and endothelium-dependent responses, Pflugers Arch. Pflugers Arch 459 (6) (2010) 881–895.
[5] A. Oni-Orisan, Y. Deng, R.N. Schuck, K.N. Theken, M.L. Edin, F.B. Lih, K. Molnar, L. DeGraff, K.B. Tomer, D.C. Zeldin, C.R. Lee, Dual modulation of cyclooxygenase and CYP epoxygenase metabolism and acute vascular inflammation in Mice, Prostagl. Other Lipid Mediat. 104–105 (2013) 67–73.
[6] B. Fisslthaler, R. Popp, L. Kiss, M. Potente, D.R. Harder, I. Fleming, R. Busse, Cytochrome P450 2C is an EDHF synthase in coronary arteries, Nature 401 (6752) (1999) 493–497, https://doi.org/10.1038/46816.
[7] S.L. Archer, F.S. Gragasin, X. Wu, S. Wang, S. McMurtry, D.H. Kim, M. Platonov, A. Koshal, K. Hashimoto, W.B. Campbell, J.R. Falck, E.D. Michelakis, Endothelium-derived hyperpolarizing factor in human internal mammary artery is 11,12-epoxyeicosatrienoic acid and causes relaxation by activating smooth muscle BK(Ca) channels, Circulation 107 (2003) 769–776.
[8] I. Fleming, U.R. Michaelis, D. Bredenkötter, B. Fisslthaler, F. Dehghani, R. P. Brandes, R. Busse, Endothelium-derived hyperpolarizing factor synthase (Cytochrome P450 2C9) is a functionally significant source of reactive oxygen species in coronary arteries, Circ. Res. 88 (2001) 44–51.
[9] M. Muñoz, M.E. López-Oliva, E. Pinilla, M.P. Martínez, A. Sánchez, C. Rodríguez, A. García-Sacristán, M. Hernández, L. Rivera, D. Prieto, CYP epoxygenase-derived H2O2 is involved in the endothelium-derived hyperpolarization (EDH) and relaxation of intrarenal arteries, Free Radical Biol. Med. 106 (2017) 168–183.
[10] C.K. Abrass, Overview: obesity: what does it have to do with kidney disease? J. Am. Soc. Nephrol. 15 (2004) 2768–2772.
[11] A.P. de Vries, P. Ruggenenti, X.Z. Ruan, M. Praga, J.M. Cruzado, I.M. Bajema, V. D. D'Agati, H.J. Lamb, D. Pongrac Barlovic, R. Hojs, M. Abbate, R. Rodriquez, C. E. Mogensen, E. Porrini, ERA-EDTA Working Group Diabesity. Fatty kidney: emerging role of ectopic lipid in obesity related renal disease, Lancet Diabetes Endocrinol. 2 (2014) 417–422.
[12] A.A. Elmarakby, J. Faulkner, M. Al-Shabrawey, M.-H. Wang, K.R. Maddipati, J. D. Imig, Deletion of soluble epoxide hydrolase gene improves renal endothelial function and reduces renal inflammation and injury in streptozotocin-induced type 1 diabetes, Am. J. Physiol. Regul. Integr. Comp. Physiol. 301 (5) (2011) R1307–R1317.
[13] G. Chen, R. Xu, Y. Wang, P. Wang, G. Zhao, X. Xu, A. Gruzdev, D.C. Zeldin, D. W. Wang, Genetic disruption of soluble epoxide hydrolase is protective against streptozotocin-induced diabetic nephropathy, Am. J. Physiol. Endocrinol. Metab. 303 (5) (2012) E563–E575.
[14] A. Dey, R.S. Williams, D.M. Pollock, D.W. Stepp, J.W. Newman, B.D. Hammock, J. D. Imig, Altered kidney CYP2C and cyclooxygenase-2 levels are associated with obesity-related albuminuria, Obes. Res. 12 (8) (2004) 1278–1289.
[15] X. Zhao, A. Dey, O.P. Romanko, D.W. Stepp, M.-H. Wang, Y. Zhou, L. Jin, J. S. Pollock, R.C. Webb, J.D. Imig, Decreased epoxygenase and increased epoxide hydrolase expression in the mesenteric artery of obese Zucker rats, Am. J. Physiol. Regul. Integr. Comp. Physiol. 288 (1) (2005) R188–R196.
[16] X. Zhao, J.E. Quigley, J. Yuan, M.H. Wang, Y. Zhou, J.D. Imig, PPAR-alpha activator fenofibrate increases renal CYP-derived eicosanoid synthesis and improves endothelial dilator function in obese Zucker rats, Am. J. Physiol. Heart Circ. Physiol. 290 (6) (2006) H2187–H2195.
[17] A. Gilani, V. Pandey, V. Garcia, K. Agostinucci, S.P. Singh, J. Schragenheim, L. Bellner, J.R. Falck, M.P. Paudyal, J.H. Capdevila, N.G. Abraham, M. Laniado Schwartzman, High-fat diet-induced obesity and insulin resistance in CYP4a14-/- mice is mediated by 20-HETE, Am. J. Physiol. Regul. Integr. Comp. Physiol. 315 (5) (2018) R934–R944.
[18] A. Soler, I. Hunter, G. Joseph, R. Hutcheson, B. Hutcheson, J. Yang, F.F. Zhang, S. R. Joshi, C. Bradford, K.H. Gotlinger, R. Maniyar, J.R. Falck, S. Proctor, M. L. Schwartzman, S.A. Gupte, P. Rocic, Elevated 20-HETE in metabolic syndrome regulates arterial stiffness and systolic hypertension via MMP12 activation, J. Mol. Cell. Cardiol. 117 (2018) 88–89.
[19] A. Soler, I. Hunter, G. Joseph, R. Hutcheson, B. Hutcheson, J. Yang, F.F. Zhang, S. R. Joshi, C. Bradford, K.H. Gotlinger, R. Maniyar, J.R. Falck, S. Proctor, M. L. Schwartzman, S.A. Gupte, P. Rocic, Elevated 20-HETE impairs coronary collateral growth in metabolic syndrome via endothelial dysfunction, Am. J. Physiol. Heart Circ. Physiol. 312 (3) (2017) H528–H540.
[20] A. Dey, C. Maric, W.H. Kaesemeyer, C.Z. Zaharis, J. Stewart, J.S. Pollock, J.D. Imig, Rofecoxib decreases renal injury in obese Zucker rats, Clin. Sci. (Lond.) 107 (6) (2004) 561–570.
[21] M. Muñoz, A. Sánchez, M. Pilar Martínez, S. Benedito, M.-E. López-Oliva, A. García-Sacristán, M. Hernández, D. Prieto, COX-2 is involved in vascular oxidative stress and endothelial dysfunction of renal interlobar arteries from obese Zucker rats, Free Radical Biol. Med. 84 (2015) 77–90.
[22] M. Muñoz, M.E. López-oliva, C. Rodríguez, M. Pilar, J. Sáenz-medina, A. Sánchez, B. Climent, S. Benedito, A. García-Sacristán, L. Rivera, M. Hernández, D. Prieto, Differential contribution of Nox1, Nox2 and Nox4 to kidney vascular oxidative stress and endothelial dysfunction in obesity, Redox Biol. 28 (2020) 101330.
[23] S.C. Khojasteh, S. Prabhu, J.R. Kenny, J.S. Halladay, A.Y. Lu, Chemical inhibitors of cytochrome P450 isoforms in human liver microsomes: a re-evaluation of P450 isoform selectivity, Eur. J. Drug Metab. Pharmacokinet. 36 (1) (2011) 1–16.
[24] N. Miyata, K. Taniguchi, T. Seki, T. Ishimoto, M. Sato-Watanabe, Y. Yasuda, M. Doi, S. Kametani, Y. Tomishima, T. Ueki, M. Sato, K. Kameo, HET0016, a potent and selective inhibitor of 20-HETE synthesizing enzyme, Br. J. Pharmacol. 133 (3) (2001 Jun) 325–329.
[25] M. Muñoz, M.P. Martínez, M.E. López-Oliva, C. Rodríguez, C. Corbacho, J. Carballido, A. García-Sacristán, M. Hernández, L. Rivera, J. Sáenz-Medina, D. Prieto, Hydrogen peroxide derived from NADPH oxidase 4- and 2 contributes to the endothelium-dependent vasodilatation of intrarenal arteries, Redox Biol. 19 (2018) 92–104.

[26] E. Pinilla, A. Sánchez, M.P. Martínez, M. Muñoz, A. García-Sacristán, R. Köhler, D. Prieto, L. Rivera, Endothelial KCa 1.1 and KCa 3.1 channels mediate rat intrarenal artery endothelium-derived hyperpolarization response, Acta Physiol. (Oxf.) 231 (4) (2021), https://doi.org/10.1111/apha.2021.231.issue-410.1111/apha.13598.
[27] L. Rivera, R. Blanco, P. de la Villa, Calcium-permeable glutamate receptors in horizontal cells of the mammalian retina, Vis. Neurosci. 18 (2001) 995–1002.
[28] B. Climent, L. Moreno, P. Martínez, C. Contreras, A. Sánchez, F. Pérez-Vizcaíno, A. García-Sacristán, L. Rivera, D. Prieto, S.-Z. Xu, Upregulation of SK3 and IK1 channels contributes to the enhanced endothelial calcium signaling and the preserved coronary relaxation in obese Zucker rats, PLoS ONE 9 (10) (2014) e109432, https://doi.org/10.1371/journal.pone.0109432.
[29] S.S. Mokhtar, P.M. Vanhoutte, S.W. Leung, M.I. Yusof, W.A. Wan Sulaiman, A. Z. Mat Saad, R. Suppian, A.H. Rasool, Endothelium dependent hyperpolarization-type relaxation compensates for attenuated nitric oxide-mediated responses in subcutaneous arteries of diabetic patients, Nitric Oxide 53 (2016) 35–44.
[30] C. Schach, M. Resch, P.M. Schmid, G.A. Riegger, D.H. Endemann, Endothelium dependent hyperpolarization-type relaxation compensates for attenuated nitric oxide-mediated responses in subcutaneous arteries of diabetic patients, Am. J. Physiol. Heart Circ. Physiol. 307 (8) (2014) H1093–H1102.
[31] J.S. Wang, H. Singh, F. Zhang, et al., Endothelial dysfunction and hypertension in rats transduced with CYP4A2 adenovirus, Circ. Res. 98 (2006) 962–969.
[32] K. Inoue, K. Sodhi, N. Puri, K.H. Gotlinger, J. Cao, R. Rezzani, J.R. Falck, N. G. Abraham, M. Laniado-Schwartzman, Endothelial-specific CYP4A2 overexpression leads to renal injury and hyper-tension via increased production of 20-HETE, Am. J. Physiol. Renal Physiol. 297 (4) (2009) F875–F884.
[33] C.-C. Wu, M.L. Schwartzman, The role of 20-HETE in androgen-mediated hypertension, Prostagl. Other Lipid Mediat. 96 (1-4) (2011) 45–53.
[34] Ü. Savas, S. Wei, M.H. Hsu, J.R. Falck, F.P. Guengerich, J.H. Capdevila, E. F. Johnson, 20-Hydroxyeicosatetraenoic Acid (HETE)-dependent Hypertension in Human Cytochrome P450 (CYP) 4A11 Transgenic Mice: normalization of blood pressure by sodium restriction, hydrochlorothiazide, or blockade of the type 1 angiotensin ii receptor, J. Biol. Chem. 291 (32) (2016) 16904–16919.
[35] J.P. Hardwick, K. Eckman, Y.K. Lee, M.A. Abdelmegeed, A. Esterle, W.M. Chilian, J.Y. Chiang, B.J. Song, Eicosanoids in metabolic syndrome, Adv. Pharmacol. 66 (2013) 157–266.
[36] I.-J. Tsai, K.D. Croft, T.A. Mori, J.R. Falck, L.J. Beilin, I.B. Puddey, A.E. Barden, 20-HETE and F2-isoprostanes in the metabolic syndrome: the effect of weight reduction, Free Radical Biol. Med. 46 (2) (2009) 263–270.
[37] Y. Issan, E. Hochhauser, A. Guo, K.H. Gotlinger, R. Kornowski, D. Leshem-Lev, E. Lev, E. Porat, E. Snir, C.I. Thompson, N.G. Abraham, M. Laniado-Schwartzman, Elevated level of pro-inflammatory eicosanoids and EPC dysfunction in diabetic patients with cardiac ischemia, Prostagl. Other Lipid Mediat. 100-101 (2013) 15–21.
[38] H. Huang, C. Morisseau, J. Wang, T. Yang, J.R. Falck, B.D. Hammock, M.-H. Wang, Increasing or stabilizing renal epoxyeicosatrienoic acid production attenuates abnormal renal function and hypertension in obese rats, Am. J. Physiol. Renal Physiol. 293 (1) (2007) F342–F349.
[39] K.N. Theken, Y. Deng, R.N. Schuck, A. Oni-Orisan, T.M. Miller, M. Alison Kannon, S.M. Poloyac, C.R. Lee, Enalapril reverses high-fat diet-induced alterations in cytochrome P450-mediated eicosanoid metabolism, Am. J. Physiol. Endocrinol. Metab. 302 (5) (2012) E500–E509.
[40] P. Toth, Z. Tucsek, D. Sosnowska, T. Gautam, M. Mitschelen, S. Tarantini, F. Deak, A. Koller, W.E. Sonntag, A. Csiszar, Z. Ungvari, Age-related autoregulatory dysfunction and cerebromicrovascular injury in mice with angiotensin II-induced hypertension, J. Cereb. Blood Flow Metab. 33 (2013) 1732–1742.
[41] R.N. Schuck, K.N. Theken, M.L. Edin, M. Caughey, A. Bass, K. Ellis, B. Tran, S. Steele, B.P. Simmons, F.B. Lih, K.B. Tomer, M.C. Wu, A.L. Hinderliter, G. A. Stouffer, D.C. Zeldin, C.R. Lee, Cytochrome P450-derived eicosanoids and vascular dysfunction in coronary artery disease patients, Atherosclerosis 227 (2013) (2013) 442–448.
[42] J. Cheng, J.-S. Ou, H. Singh, J.R. Falck, D. Narsimhaswamy, K.A. Pritchard, M. L. Schwartzman, 20-hydroxyeicosatetraenoic acid causes endothelial dysfunction via eNOS uncoupling, Am. J. Physiol. Heart Circ. Physiol. 294 (2) (2008) H1018–H1026.
[43] J. Cheng, C.C. Wu, K.H. Gotlinger, F. Zhang, J.R. Falck, D. Narsimhaswamy, M. L. Schwartzman, 20-hydroxy-5,8,11,14-eicosatetraenoic acid mediates endothelial dysfunction via IkappaB kinase-dependent endothelial nitric-oxide synthase uncoupling, J. Pharmacol. Exp. Therap. 332 (2010) 57–65.
[44] A.M. Guo, A.S. Arbab, J.R. Falck, P. Chen, P.A. Edwards, R.J. Roman, & Scicli AG Activation of vascular endothelial growth factor through reactive oxygen species mediates 20-hydroxyeicosatetraenoic acid-induced endothelial cell proliferation, J. Pharmacol. Exp. Therap. 321 (2007) 18–27.
[45] M. Medhora, Y. Chen, S. Gruenloh, D. Harland, S. Bodiga, J. Zielonka, D. Gebremedhin, Y. Gao, J.R. Falck, S. Anjaiah, E.R. Jacobs, 20-HETE increases superoxide production and activates NAPDH oxidase in pulmonary artery endothelial cells, Am. J. Physiol. Lung Cell. Mole. Physiol. 294 (5) (2008) L902–L911.
[46] T. Ishizuka, J. Cheng, H. Singh, M.D. Vitto, V.L. Manthati, J.R. Falck, M. Laniado-Schwartzman, 20-Hydroxyeicosatetraenoic acid stimulates nuclear factor-kappaB activation and the production of inflammatory cytokines in human endothelial cells, J. Pharmacol. Exp. Therap. 324 (2008) 103–110.
[47] P. Rocic, M.L. Schwartzman, 20-HETE in the regulation of vascular and cardiac function, Pharmacol. Ther. 192 (2018) 74–87.
[48] N.C. Ward, I.B. Puddey, J.M. Hodgson, L.J. Beilin, K.D. Croft, Urinary 20-hydroxyeicosatetraenoic acid excretion is associated with oxidative stress in hyper-tensive subjects, Free Rad. Biol. Med. 38 (2005) (2005) 1032–1036.
[49] N.C. Ward, J. Rivera, J. Hodgson, I.B. Puddey, L.J. Beilin, J.R. Falck, K.D. Croft, Urinary 20-hydroxyeicosatetraenoic acid is associated with endothelial dysfunction in humans, Circulation 110 (2004) 438–443.
[50] A.A. Eid, Y. Gorin, B.M. Fagg, R. Maalouf, J.L. Barnes, K. Block, H.E. Abboud, Mechanisms of podocyte injury in diabetes: role of cytochrome P450 and NADPH oxidases, Diabetes 58 (5) (2009) 1201–1211.
[51] N. Villalba, P. Martínez, A.M. Bríones, A. Sánchez, M. Salaíces, A. García-Sacristán, M. Hernández, S. Benedito, D. Prieto, Differential structural and functional changes in penile and coronary arteries from obese Zucker rats, Am. J. Physiol. Heart Circ. Physiol. 297 (2) (2009) H696–H707.